Inorganic Chemistry

Article

pubs.acs.org/IC

Mechanistic Insight into Electrocatalytic H_2 Production by $[Fe_2(CN)\{\mu\text{-}CN(Me)_2\}(\mu\text{-}CO)(CO)(Cp)_2]$: Effects of Dithiolate Replacement in [FeFe] Hydrogenase Models

Federica Arrigoni,[†] Luca Bertini,[†] Luca De Gioia,[†] Andrea Cingolani,[‡] Rita Mazzoni,[‡] Valerio Zanotti,*[,‡] and Giuseppe Zampella*[,†]

[†]Department of Biotechnology and Biosciences, University of Milan-Bicocca, Piazza della Scienza 2, 20126 Milan, Italy

[‡]Department of Chimica Industriale "Toso Montanari", University of Bologna, V. le Risorgimento 4, 40136 Bologna, Italy

Supporting Information

ABSTRACT: DFT has been used to investigate viable mechanisms of the hydrogen evolution reaction (HER) electrocatalyzed by $[Fe_2(CN)\{\mu\text{-}CN(Me)_2\}(\mu\text{-}CO)(CO)(Cp)_2]$ (**1**) in AcOH. Molecular details underlying the proposed ECEC electrochemical sequence have been studied, and the key functionalities of CN^- and amino-carbyne ligands have been elucidated. After the first reduction, CN^- works as a relay for the first proton from AcOH to the carbyne, with this ligand serving as the main electron acceptor for both reduction steps. After the second reduction, a second protonation occurs at CN^- that forms a Fe(CNH) moiety: i.e., the acidic source for the H_2 generation. The hydride (formally $2e/H^+$), necessary to the heterocoupling with H^+ is thus provided by the μ-$CN(Me)_2$ ligand and not by Fe centers, as occurs in typical $L_6Fe_2S_2$ derivatives modeling the hydrogenase active site. It is remarkable, in this regard, that CN^- plays a role more subtle than that previously expected (increasing electron density at Fe atoms). In addition, the role of AcOH in shuttling protons from CN^- to $CN(Me)_2$ is highlighted. The incompetence for the HER of the related species $[Fe_2\{\mu\text{-}CN(Me)_2\}(\mu\text{-}CO)(CO)_2(Cp)_2]^+$ (2^+) has been investigated and attributed to the loss of proton responsiveness caused by CN^- replacement with CO. In the context of hydrogenase mimicry, an implication of this study is that the dithiolate strap, normally present in all synthetic models, can be removed from the Fe_2 core without loss of HER, but the redox and acid−base processes underlying turnover switch from a metal-based to a ligand-based chemistry. The versatile nature of the carbyne, once incorporated in the Fe_2 scaffold, could be exploited to develop more active and robust catalysts for the HER.

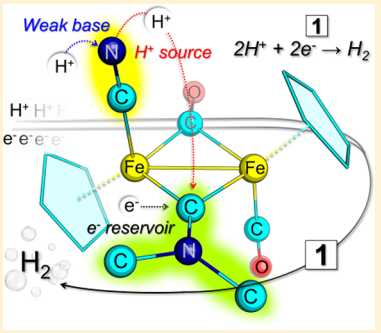

INTRODUCTION

Due to their similarities with the [FeFe]-hydrogenase active site (Scheme 1, **I**), diiron dithiolato carbonyls (Scheme 1, set of compounds **II**) have been the subject of intense research activities in the past decade which strongly contributed to a better understanding of structural and mechanistic aspects of [FeFe]-H_2ases.[1,2] Interest toward diiron dithiolate model systems is also driven by the need to address a fundamental issue in the use of H_2 as an energy vector: the replacement of platinum (and other noble metals) with catalysts based on abundant and sustainable metals such as iron.[3] On the basis of the reasonable assumption that diiron complexes resembling the active site of natural [FeFe]-H_2ases might act as effective electrocatalysts for H_2 production, a huge number of diiron mimics have been designed by modification of the bridgehead group or substitution of carbonyls and cyanides with other ligands.[4−8] In spite of the considerable efforts, the development of efficient electrocatalysts for H_2 production based on [FeFe]-H_2ases mimics is still far from being fully accomplished. Extension of the research field into a broader area involving diiron complexes not necessarily restricted to dithiolate mimics would potentially provide more chances to develop new and efficient catalysts. In other words, going beyond the "dithiolate paradigm", but still taking advantage of possible cooperative effects associated with the presences of two adjacent Fe atoms, should provide access to electrocatalytic H_2 production based

Scheme 1

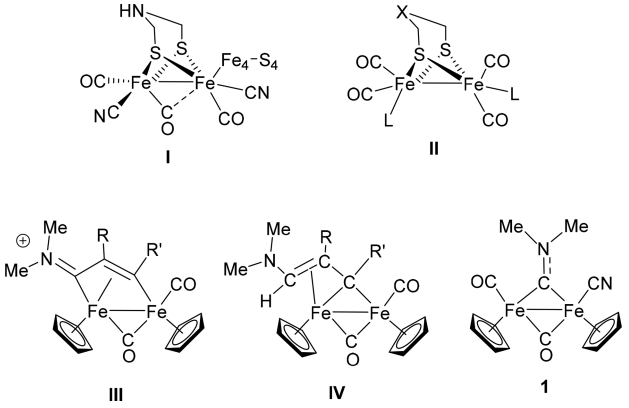

Received: August 3, 2017
Published: November 7, 2017

DOI: 10.1021/acs.inorgchem.7b01954
Inorg. Chem. 2017, 56, 13852−13864

on a mechanism not so strictly related to those of [FeFe]-H_2ases. With this idea in mind we have recently investigated a number of diiron organometallic complexes containing cyclopentadienyls (η^5-C_5H_5, Cp), bridging and/or terminal CO, and bridging hydrocarbyl ligands such as alkynyl, alkenyl, allyl, allenyl, vinyliminium (Scheme 1, compound **III**), and vinylalkylidene (Scheme 1, compound **IV**) as potential electrocatalysts for H_2 production.[9] The presence of Cp ligands produce effects comparable, at least in terms of electron donor ability, to those of other ligands (e.g., phosphines, isocyanides, carbenes) generally used to replace CO in dithiolate mimics.[10] In our case, the most relevant change is the replacement of bridging dithiolate or aza-dithiolate ligands with bridging hydrocarbyl ligands, in that aza-dithiolate ligands are recognized to have a major role in H_2ases,[11,12] as well as in model systems.[13−20]

We found that in a limited number of cases diiron complexes, namely those containing a bridging carbyne (e.g., complex **1**, Scheme1), can act as electrocatalysts for H_2 generation, affording results comparable to those of many common dithiolate systems (TON 15.5 for complex **1**).[9] It was not clear why these, unlike other diiron hydrocarbyl complexes, were effective in providing a catalytic pathway to proton reduction. In particular, it was surprising that complexes with the most structured bridging ligands, incorporating π-extended systems and heteroatoms, such as vinyliminium **III** and vinylalkylidenes **IV**, in principle better candidates to mimic the behavior of bridging azadithiolate, were ineffective as catalysts. Indeed, on the basis of chemical and electrochemical evidence we came to the conclusion that these bridging ligands were detrimental to catalysis in that reduction and protonation events occurred at the ligand, in place of the metal, therefore inhibiting a fundamental step in the sequence required to generate H_2. Our preliminary screening work also evidenced that only carbyne complexes containing a CN^- ligand gave significant catalysis. A reasonable but general explanation is that only a specific combination of ligands can provide a favorable electron density at the Fe−Fe core to favor metal protonation without shifting the reduction potentials to very negative values, which is disadvantageous. However, cyanide might have a specific role in the rather complex sequence of steps involved in the catalytic H_2 production in that replacing cyanide ligand by CO in the complex $[Fe_2\{\mu\text{-}CN(Me)_2\}(\mu\text{-}CO)(CO)_2(Cp)_2]^+$ (hereafter $\mathbf{2}^+$) results in a complete loss of H_2 evolution reactivity (HER). DFT has been thus used to address this crucial difference, through the characterization of possible reaction mechanisms associated with H_2 production at a molecular level.

COMPUTATIONAL DETAILS

DFT calculations have been carried out by the Turbomole 7.1.1 suite of programs.[21] The GGA BP86-RI functional[22] has been used in conjunction with the split-valence polarized basis TZVP[23] on all atoms, thus explicitly considering also the core electrons of Fe. This computational scheme turned out to reliably model several features related to diiron hydrogenase mimics.[24−29]

BP86 has also been reported to outperform the more popular B3LYP[30] in the theoretical reproduction of the redox potentials of Fe_2 complexes modeling hydrogenase, which is a crucial aspect when studying the electrocatalytic behavior of these compounds.[31] The results herein confirm the previously reported data (vide infra).

Nonetheless, the selected theory level has been herein further validated by comparing simulated structural parameters vs available XRD geometries and also theoretical vs experimental reduction potentials. Moreover, with the aim of corroborating the information emerging from our computations, the energy profiles associated with the HER have been recomputed also by means of other functionals such as the aforementioned B3LYP (Table S5 in the Supporting Information), and the meta-GGA M06[32] has been used to test possible better performance in reproducing structural parameters.

The solvent has been modeled according to the COSMO approach, which considers the solvent as a dielectric continuum (with ε = 37.5; acetonitrile).[33]

Transition state structures have been searched through an analytical Hessian (or pseudo-Newton−Raphson) procedure entailing an initial preoptimization of a guess of transition state, continued through an eigenvector following step.[34] Atomic partial charges have been evaluated by natural bond orbital (NBO) methods.[35]

The Fc/Fc^+ redox potential (−4.87 V; acetonitrile) has been used as a reference to scale the absolute reduction potentials. Indeed, computation of reduction potentials is based on the free energy difference (in solution) between reduced and oxidized species, $\Delta G^\circ_{solv} = G^\circ(ox)_{solv} - G^\circ(red)_{solv}$, through the equation $\Delta G^\circ_{solv} = -nFE^\circ$, where n is the number of electrons involved in the reduction and F is the Faraday constant (23.061 kcal mol^{-1} V^{-1}). In order to obtain free energy, the KS-SCF electronic energy (E_{solv}) has been corrected by enthalpy and entropy contributions at 298.15 K and 1 bar (BP86 scaling factor 0.9914). In some cases, the use of ΔE_{solv} provided a better match to experimental data than ΔG°_{solv} and the reasons for such an apparent anomaly have been recently discussed and clarified in a paper on DFT modeling of the redox behavior of [FeFe]-hydrogenase models.[36]

RESULTS AND DISCUSSION

Characterization of 1 and 2^+. The main geometrical parameters of possible isomers of the amino-carbyne complexes **1** and $\mathbf{2}^+$ are shown in Table 1, along with those of $[Fe_2(\mu\text{-}CNMe_2)(\mu\text{-}CO)(CO)(CH_2CN)(Cp)_2]$ (**1(CH$_2$CN)**), an analogue of **1**.[37] The labels "**a**" and "**b**" denote the reciprocal trans/cis disposition of the Cp ligands. The very good match between XRD[37] and DFT parameters confirmed the selected computational method as suitable to describe the molecular species under investigation (the XRD vs DFT discrepancy is on the order of 0.02 Å and B3LYP AND M06 provided 0.04 and 0.03 Å, respectively; see Figure S1 and Table S1 in the Supporting

Table 1. Most Relevant DFT Interatomic Distances of 1, 2^+, and 1(CH$_2$CN) and X-ray Data of 1(CH$_2$CN)[a]

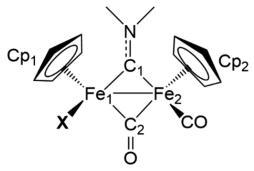

1a X = CN⁻
2a⁺ X = CO
1(CH$_2$CN) X = CH_2CN^-

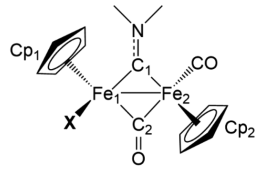

1b X = CN⁻
2b⁺ X = CO

	1a	1b	$2a^+$	$2b^+$	1(CH$_2$CN)	1(CH$_2$CN) XRD
$Fe_1\cdots Fe_2$	2.531	2.513	2.538	2.543	2.516	2.502
$Fe_1\cdots C_2$	2.022	2.013	1.942	1.945	2.029	2.003
$Fe_2\cdots C_2$	1.859	1.859	1.944	1.946	1.844	1.852
$Fe_1\cdots C_1$	1.878	1.884	1.877	1.877	1.889	1.886
$Fe_2\cdots C_1$	1.829	1.835	1.878	1.878	1.833	1.843
$Fe_1\cdots Cp_1$ (av)	2.155	2.147	2.150	2.157	2.150	2.100
$Fe_2\cdots Cp_2$ (av)	2.155	2.150	2.151	2.157	2.150	2.120

[a]Distances in Å.

DOI: 10.1021/acs.inorgchem.7b01954
Inorg. Chem. 2017, 56, 13852−13864

Information for optimized structures and geometrical parameters).

In terms of electron counting, although bridging carbynes (alkylidynes) are generally considered as neutral three-electron donors, in the case of the bridging amino-carbyne complexes, these are more conveniently considered as μ-CNRR′$^{+}$ (iminium, two-electron donor). This accounts for the relatively short μ-C−N bond distance (about 1.30 Å) and is also consistent with a formal Fe^{I}_{2} oxidation state.

X-ray analysis revealed that **1(CH$_2$CN)** features the Cp ligands in a mutual cis orientation and the CN$^-$ group in a terminal position at Fe. A trans disposition of Cp groups and the Fe terminal position of the CN$^-$ ligand are instead preferred in **1**, since (i) **1a** is predicted to be slightly more stable (by 0.6 kcal/mol, Table S2 in the Supporting Information) than **1b** and (ii) isomers featuring bridging cyanide are ∼10 kcal/mol higher in energy than the ground state. In **2**$^+$, instead, the cis isomer is predicted to be 0.4 kcal/mol more stable than the trans isomer. Since the energetic differences between cis and trans isomers of both complexes are far below the accuracy limit of DFT, it can be concluded that there is not a clear preferential disposition of the Cp ligands in the class of compounds under investigation.

These results are consistent with previously reported observations concerning the cis/trans isomeric composition of related complexes of the type [Fe$_2${μ-CN(Me)R}(μ-CO)(CO)(X)(Cp)$_2$] (X = halides and pseudohalides).[38]

Mechanistic Dissection of the ECEC Electrochemistry of HER. *Reduction of 1 and 2*$^+$ *(ECEC).* The first event of HER catalyzed by **1** (**2**$^+$ is catalytically incompetent) is a one-electron reduction. This clearly emerges from CV data, which indicate an ECEC mechanism, already reported about some Fe_2S_2 H_2ase models.[39−41]

The thermodynamic speciation of products formed by one-electron reduction of **1** and **2**$^+$ has been necessary to compute DFT reduction potentials, which have been subsequently compared to CV parameters (see Table 2 for experimental vs theoretical comparison and Figures S6 and S7 in the Supporting Information for visual inspection of reduced isomers). The experimental vs theoretical agreement is satisfying (the largest discrepancy is only 40 mV) and constitutes a further validation of the adopted density functional (BP86) for the purposes of the present investigation (even in comparison to other DFT methods such as B3LYP, see Table 2).

Table 2. DFT vs Experimental Reduction Potentials

	$E_{red1}°$ (V)	
	1 → **1**$^-$	**2**$^+$ → **2**
BP86/TZVP/COSMO	−2.08	−1.36
B3LYP/TZVP/COSMO	−1.60	−0.92
exptl[a]	−2.04	−1.40

[a]Experimental values are reported in ref 9.

One-electron reduction of **1a**, **1b**, **2a**$^+$, and **2b**$^+$ yielded **1a**$^-$, **1b**$^-$, **2a**, and **2b**, respectively, with all species retaining the original Cp group's configuration. The most relevant geometrical parameters of each reduced isomer are presented in Table S3 in the Supporting Information. A general concomitant elongation of the Fe−Fe, Fe−Cp, and Fe−$C_{carbyne}$ distances upon reduction of both **1** and **2**$^+$ has been observed. These structural variations can be rationalized on the basis of both the LUMO shape of **1** and **2**$^+$ (that indicates the atoms mostly involved in the reduction process) and the partial charge difference between the reduced and the oxidized forms (that evidences the charge redistribution in the product). In this class of compounds, the LUMO is antibonding with respect to Fe−Fe, since featuring a σ* symmetry with a predominant d_{z^2} character (see Figure 10 and Figure S2 in the Supporting Information). Furthermore, NBO analysis (Table S4 in the Supporting Information) suggests that the additional electron is mostly located on Cp ligands and to a lesser extent on the aminocarbyne group. Regarding energetics, it is worth mentioning that the relative stability of cis vs trans isomers is not affected by first electron transfer, remaining always very close to zero (see Table S2 in the Supporting Information).

A comparison of the partial charges of Fe atoms in **1** vs **2**$^+$ (i.e., before reduction) shows an interesting and counterintuitive result: all metal ions bear a very slightly positive charge (close to zero). Aside from the poorly informative intrinsic value of the Fe charge, the unexpected electron density equivalence between the metallic centers of the neutral (and with coordinating CN$^-$) and cationic species is notable. Indeed, it was postulated that cyanide might increase the electron density at the diiron core, thus favoring its protonation, an essential step in the electrocatalytic proton reduction.[9] A similar role for cyanide was also proposed for diiron dithiolates bearing at least another σ-donor ligand along with cyanide.[42] In light of the present observation, a more elusive role played by cyanide has to be envisaged to justify the HER detection in **1** but not in **2**$^+$ (vide infra).

Protonation of 1$^-$ *and 2 (ECEC).* A protonation event (C) is invoked after reduction of **1** and **2**$^+$, as evidenced by CV. The protonation process of **1**$^-$ by CH_3CO_2H in acetonitrile has been thus dissected from both kinetic and thermodynamic standpoints (see Figures 1 and 2 for results on protonation of **1**$^-$ and Figure 3 for results related to protonation of **2**). Further, with the aim of investigating whether the redox state of the complex could affect the regiochemistry of protonation, we have extended the speciation study performed for **1**$^-$ (→**1H**) also to **1** (→**1H**$^+$) and **1**$^{2-}$ (→**1H**$^-$). The comparison is shown in Figure 2.

It is fair to point out that protonation of neither **1** nor **1**$^{2-}$ is compatible with the ECEC mechanism under investigation. Nonetheless, on the one hand **1H**$^+$ might be relevant for future investigations involving the use of stronger acids (stronger than AcOH, such as CF_3SO_3H or HBF_4·Et_2O) and, on the other hand, an initial double reduction (with subsequent protonation) could be observed in variants of **1** featuring stronger acceptor ligands. Indeed, initial two-electron reduction has been already reported for a series of electron-poor $Fe_2(CO)_6(SR)_2$ in separate contributions by the Darensbourg,[43] Glass/Evans/Lichtenberger,[44] and Weigand/Schollhammer[45] groups.

The trans isomer of **1**$^-$ has been considered as starting point for catalysis, since DFT predicts that it is the most stable structure. Such a disposition of Cp groups has been retained along the whole catalytic pathway, since this class of compounds is reported not to easily undergo cis/trans and terminal/bridging rearrangements.[46,47]

All of the putative basic sites have been systematically considered for protonation, namely cyanide N in **1Ha**, Cp C atoms in **1Hb**, terminal CO C atoms in **1Hc**, carbyne C atoms in **1Hd** and **1He** (reciprocally differing in the "face" of the catalyst involved in protonation), Fe coordinated by CN$^-$ in **1Hf**, and Fe coordinated by CO in **1Hg**. As expected from the

DOI: 10.1021/acs.inorgchem.7b01954
Inorg. Chem. 2017, 56, 13852−13864

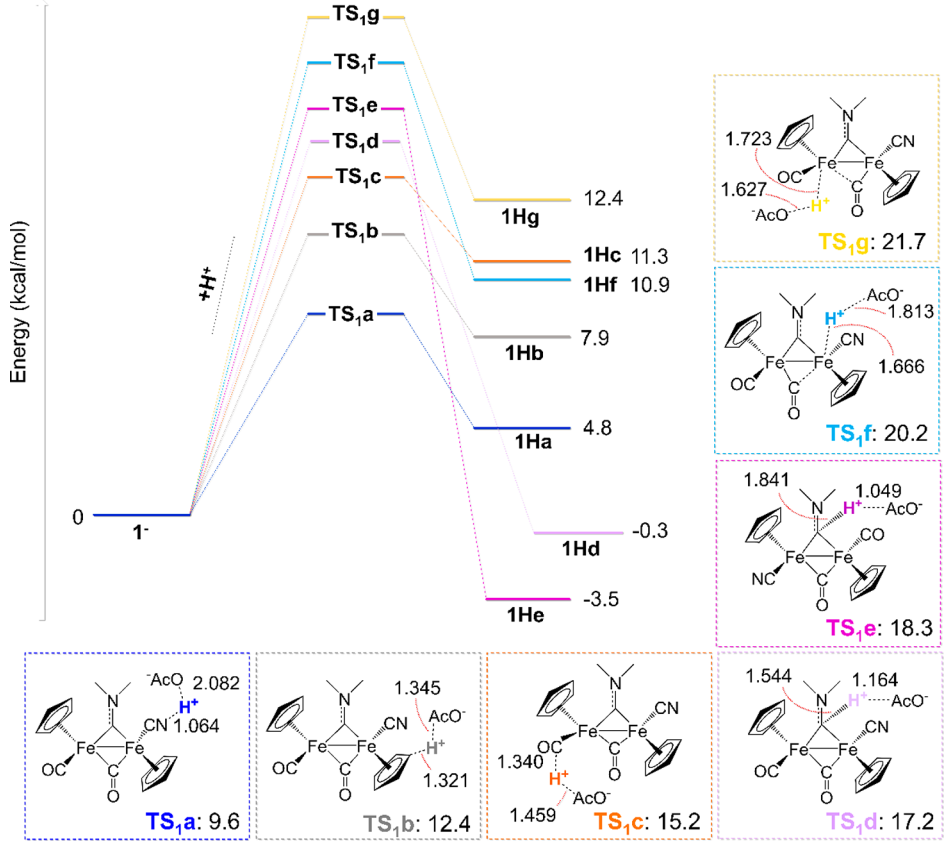

Figure 1. Energy profiles associated with $\mathbf{1}^-$ protonation. The subscript 1 designates the first of two protonation events occurring in the ECEC mechanism. The labels a, b, ... denote the various basic sites that have been considered for protonation. Transition states (TS) of $\mathbf{1}^-$ protonation by acetic acid, along with the corresponding activation barriers (kcal/mol), are also presented. The distances describing the reaction coordinate are also displayed (Å).

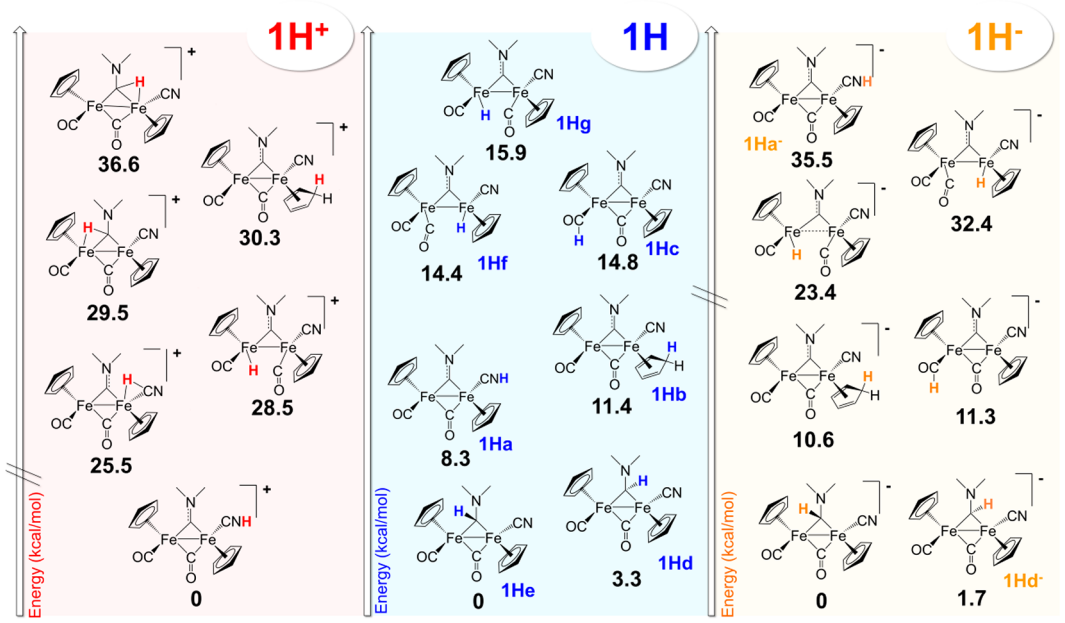

Figure 2. Thermodynamic speciation of $\mathbf{1H}^+$, **1H**, and $\mathbf{1H}^-$ species. Energies are in kcal/mol. Labels refer to the protonation energy profiles presented in Figure1.

electronic structure of the amino-carbyne ligand (see Characterization of **1** and $\mathbf{2}^+$), the carbyne $N(Me)_2$ functionality is not available as a protonation site. Indeed, its protonation resulted in a high-energy species (+30.1 kcal/mol with respect to **1H** ground state, **1He**) and the related energy profile has been excluded from Figure 1.

The kinetically preferred site for protonation is N_{CN^-} ($\mathbf{TS1_a}$ = 9.6 kcal/mol, Figure 1), although **1Ha** is not the

DOI: 10.1021/acs.inorgchem.7b01954
Inorg. Chem. 2017, 56, 13852−13864

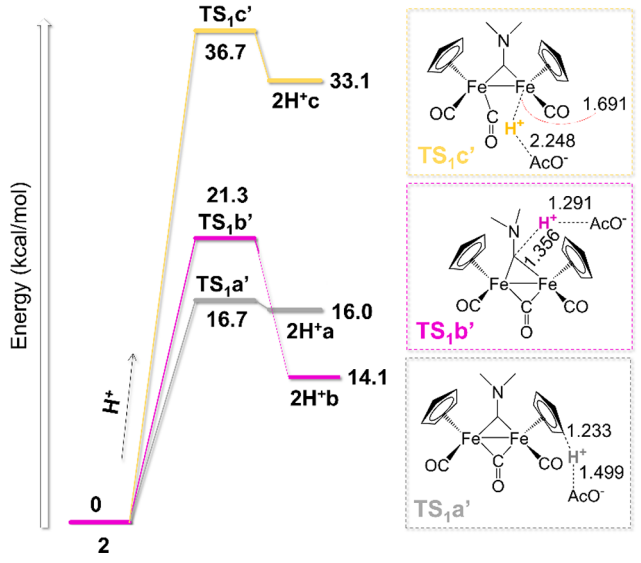

Figure 3. (left) Energy profiles associated with protonation of **2**. The subscript 1 refers to the first protonation event. The labels a, b, ... denote, instead, the various basic sites that have been considered for protonation. Energy values are given in kcal/mol. (right) Transition state structures and interatomic distances (Å) forming the reaction coordinate.

thermodynamically preferred isomer among the 1e/**1H**$^+$ species **1H** (Figures 1 and 2). Interestingly, protonation of **1** is unambiguously predicted to occur at N_{CN^-}, as all the other protonated structures are 28−41 kcal/mol higher in energy (Figure 2). Indeed, N protonation of metal-coordinated cyanides is the usual method to obtain hydrogen isocyanide complexes.[48] The present calculations predict that the first reduction makes CN^- less basic than the amino-carbyne, which results in the thermodynamically preferred site for protonation of **1**$^-$.

In addition, also protonation at Fe and Cp becomes *relatively* more favored (in comparison to that observed in neutral species) after the first one-electron reduction. Indeed, the LUMO localization in **1** had essentially shown (see Figure 10 and related discussion in Reduction of 1 and 2+ (ECEC)), that the incoming electron density is predicted to be more distributed on μ-$CN(Me)_2$ (and especially Cp groups) than on CN^- (in this regard see also **1**−**1**$^-$ NBO charge differences in Figure 10 and Table S4 in the Supporting Information). These findings indicate that reduction of the complex can affect the basic properties of the single ligands (as well as those of metals), therefore controlling of the entire regiochemistry of protonation.

Thermodynamically, protonation at CN^- is *moderately* endergonic whereas that at μ-$CN(Me)_2$ is *moderately* exergonic (Figure 1, 2). This is the typical behavior of a well optimized catalyst: it is worth recalling that too stable intermediates are as detrimental to catalysis as too high energy intermediates. Raugei and Bullock reported on examples related to such issue applied to catalysis of proton reduction.[49,50]

Both **1Hf** and **1Hg** feature a terminal hydride, while no stable Fe−Fe bridging hydrides have been detected. Indeed, in **1H**$^+$, **1H**, **2H**$^{2+}$, and **2H**$^+$, Fe_2 bridging hydrides can be only obtained as cis isomers and are always less stable than isomers terminally bound at Fe.

Energy profiles associated with protonation of **2** are presented in Figure 3, along with the corresponding transition state structures. The cis isomer of **2** has been used in computations since (i) DFT suggested that it is the most stable Cp disposition and (ii) similar diiron aminocarbyne complexes with all-CO ligands have been mostly isolated in this configuration.[46]

Unlike that of **1**$^-$, protonation of **2** by AcOH is predicted to be *significantly* endergonic for any possible basic site (even protonation at the aminocarbyne, which leads to the **2H**$^+$ ground state). Also kinetically, protonation of **2** appears to be a less favored process in comparison to the analogue computed for **1**$^-$ (activation barriers: 16.7 kcal/mol in **2** vs 9.6 kcal/mol in **1**$^-$). In general, all transition states and protonation products are much higher in energy than those obtained with **1**$^-$. This could partially be due to the overall negative charge of **1**$^-$, which makes it generally more susceptible to protonation vs a neutral species. In addition, the presence of a strong σ donor (CN^-) might suggest that the Fe−Fe bond in **1**$^-$ is more basic, although our data show (see above) that protonation at Fe is not favored in any case. Concisely, the unfavorable kinetic and thermodynamic behavior predicted by DFT for the protonation occurring after reduction in **2**$^+$ appears to be the first clue to justify the absence of HER in this derivative, thus highlighting the importance of cyanide in catalysis.

One-electron reduction significantly affects the protonation behavior of **2**$^+$, as observed in **1**. As a result, a digression on how the protonation properties can vary upon reduction in the **2**$^+$ case may be of general interest also for possible indirect implications in the H_2ase mimicry.

Actually, the most stable isomer of **2H**$^{2+}$ (0e/1H$^+$, not to be ruled out under strong acid conditions) features the hydride ligand in a bridging position between Fe and C of the amino-carbyne ligand (see Figure S3 in the Supporting Information). In addition, it is worth noting that **2H**$^{2+}$ Fe terminal hydrides are quite close in energy to the ground state (3−5 kcal/mol higher). Moreover, they are predicted to be relatively much more stable than their Fe−Fe bridging counterparts (by ∼10 kcal/mol). It may be interesting to recall that most Fe_2S_2-containing biomimics show a different behavior. Indeed, it is well-known that even Fe_2 dithiolates which feature kinetic protonation at a single Fe inescapably isomerize (more or less rapidly) to the thermodynamically stable Fe−Fe bridging hydrides, through a unimolecular rearrangement.[51,52] Bridging hydrides of Fe_2S_2 derivatives are reported to be less reactive[53] or unreactive[54] in comparison to terminal hydrides toward the HER, although the Me−H−Me fragment is recurrent in Nature and associated with reactivity in enzymes (such as nitrogenases and [Ni−Fe] hydrogenases). In contrast, Rauchfuss, Hammes-Schiffer, and Wang have very recently investigated a Cp-containing bridging Fe_2 hydride that proved to be a superior electron donor in comparison to the terminal counterpart and also a stable terminal Fe−H.[55] The neutral charge of this last (vs the typical cationic nature of previous examples) is proposed to be a crucial factor in this case.

DFT predictions on **2H**$^{2+}$ are also consistent with experimental observations in that it has been reported that the complex $[Fe_2\{\mu\text{-}CN(Me)_2\}(\mu\text{-}CO)(CO)(NCCH_3))\text{-}(Cp)_2]^+$, which is obtained by **2**$^+$ replacing CO with the more labile $NCCH_3$ ligand, reacts with $NaBH_4$. Replacement of the acetonitrile ligand takes place, but instead of a terminal hydride, a bridging hydride compound is formed, which is reported to be rather stable and unreactive.[56]

Second Reduction (ECEC). As mentioned earlier, the kinetic product of **1**$^-$ protonation (**1Ha**) is different from the

DOI: 10.1021/acs.inorgchem.7b01954
Inorg. Chem. 2017, 56, 13852−13864

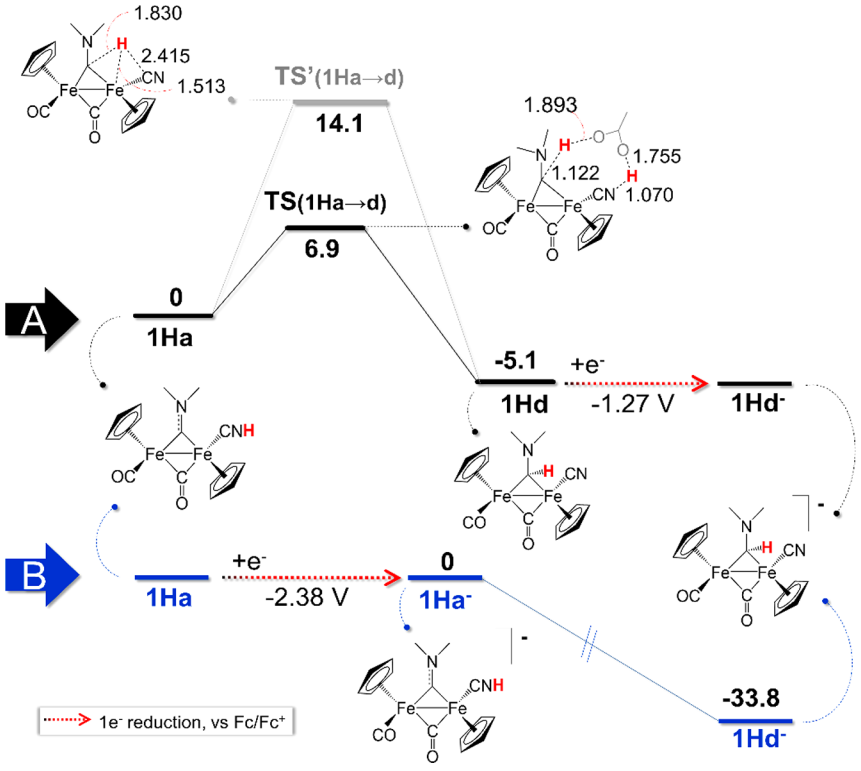

Figure 4. Representation of the second reductive event of the ECEC picture: (A) an intramolecular H^+ transfer occurs prior to reduction; (B) an intramolecular H^+ transfer occurs after reduction. Relative energy values are given in kcal/mol and distances in Å.

thermodynamic product (**1Hd**). This fact paves the way to two possible scenarios associated with the second reduction (pathways A and B) that are presented in Figure 4.

According to pathway A, **1Ha** isomerizes to the most stable tautomer **1Hd**. The isomerization can in principle occur through an intramolecular proton migration, (activation barrier 14.1 kcal/mol (**TS′1Ha→d**)). The related transition state is characterized by the assistance of one Fe center, which mediates the N-to-C proton migration. However, the assistance of an acid molecule acting as a proton shuttle affords a more rapid H^+ migration process (activation barrier 6.9 kcal/mol (**TS′1Ha→d**)). After isomerization, **1Hd** is reduced to **1Hd**$^-$ (still featuring a bridging carbene), which is the most stable **1H**$^-$ isomer.

Following pathway B, reduction of **1H** occurs prior to the intramolecular proton transfer: the one-electron reduction of **1Ha** to **1Ha**$^-$ is in fact followed by **1Ha**$^-$ isomerization to **1Hd**$^-$ (which is ∼30 kcal/mol lower in energy), a rearrangement that is predicted to be barrierless.

Notably, the reduction event following the isomerization is far more favorable than reduction prior to isomerization, suggesting that the tautomerization can trigger the second reduction.

The carbene nature of the intermediate **1Hd**$^-$ is the result of an overall transformation in which the carbyne complex **1** has stored electron density and one H^+, namely the essential ingredients for the HER, along with another proton. In this regard, it is worth noting that amino-carbyne complexes similar to **1** (e.g., $[Fe_2\{\mu\text{-CN(Me)R}\}(\mu\text{-CO})(CO)_2(Cp)_2]^+$, R = Me,[57] R = C(O)SEt[58]) are known to undergo H^- addition at the bridging carbyne to form the corresponding carbene complexes.[57,58]

Independently of which of the two routes is actually followed, the product of the second reduction is unambiguously **1Hd**$^-$. At this stage, in fact, protonated isomers at one Cp ring, at one Fe center, or at CN^- are predicted to be ∼10, ∼ 20, and ∼31 kcal/mol, respectively. This confirms that the reduction level of the complex unequivocally stabilizes species protonated at carbyne (i.e., carbenic forms) with respect to all other (2e/**1H**$^+$) species.

Second Protonation (ECEC). The protonation of **1Hd**$^-$ is illustrated in Figure 5. Protonation of the cyanide is kinetically and thermodynamically very favored. Indeed, **1HHa** is the lowest energy structure among the 2e/**2H**$^+$ **1HH** species. Interestingly, upon the second reduction, the Fe terminal hydride (in particular that at the Fe coordinated by CN^-, the only t-H found for the **1HH** state), becomes relatively more stable than the isomer protonated at Cp (by 4.6 kcal/mol). Two other hydride coordination modes to Fe have been found: a Fe−$C_{carbyne}$ μ-H, which is 10.5 kcal/mol less stable than **1HHa**, and an Fe−Fe μ-H, which instead is almost isoenergetic with **1HHa** and predicted to be more stable than t-H by 8.1 kcal/mol. This is the first time along the ECEC-related pathway that a trans Fe−H−Fe isomer has computationally been predicted to be more stable than t-H; therefore, a possible isomerization between the two forms may be expected (vide infra).

HER Mechanisms. After a second protonation **1** has overall stored two electrons and two protons and is thus activated for H_2 production. Despite the fact that the [FeFe]-H_2ase and some of the synthetic dithiolate models[5,18,59] evolve H_2 at the **2H**$^+$/1e state (with a second reduction regenerating the original form of the catalyst), we have not considered such a possibility, because of its incompatibility with the experimental data and the ECEC electrochemical sequence.

DOI: 10.1021/acs.inorgchem.7b01954
Inorg. Chem. 2017, 56, 13852−13864

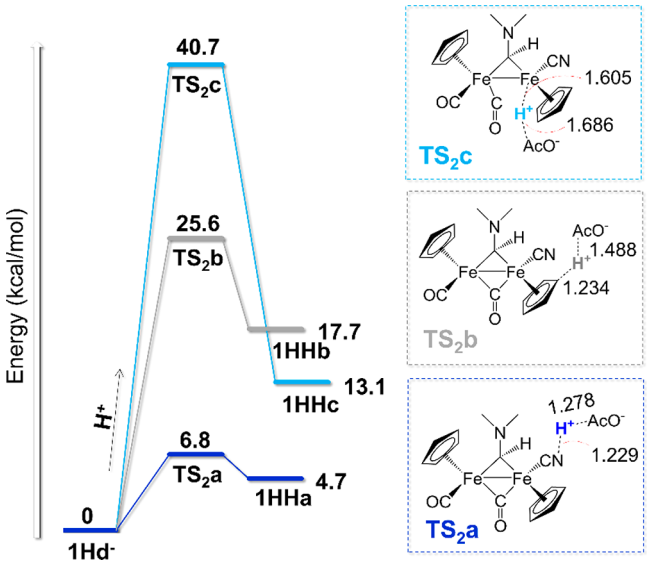

Figure 5. (left) Energy profiles associated with $\mathbf{1Hd}^-$ protonation. The subscript 2 refers to the second protonation event. The labels a, b, ... denote, instead, the various basic sites that have been considered for protonation. Energy values are given in kcal/mol. (right) Transition state structures and their main geometrical parameters. Distances are given in Å.

Thus, a concerted mechanism for H_2 formation−release has been investigated, starting from **1HHa**. As **1HHa** does not feature a metal hydride (which is normally the H^- source of the $H^- + H^+ \rightarrow H_2$ heterocoupling process), a transition state has been searched along a reaction coordinate entailing FeCN-H as an H^+ donor and μ-C(H)NMe_2 as an H^- donor to form dihydrogen (Figure 6, black pathways; see Figure 7 for visual inspection of structures related to the pathway). The activation barrier for the direct-intramolecular $H^-_{carbene}/H^+_{CN}$ heterocoupling is high (37.8 kcal/mol; Figure 6, **TS(1HHa→1+H_2)**). However, when an explicit AcOH molecule working as a proton shuttle is included in the simulation, the activation energy is dramatically lowered (26.4 kcal/mol, Figure 6, **TS′(1HHa→1+H_2)**). Such a value is in line with H_2 release near room-temperature conditions. The assistance of acid molecules in proton migration processes has been recently reported in a study on $Fe_2\{\mu\text{-}CH_2(CH_2S)_2]\}(CNR)_6$.[60]

Subsequently, we have investigated the energetic viability of other multistep mechanisms in alternative to the single-step H_2 evolution from **1HHa** (previously described). Concerning this point, it is worth mentioning that formation of Fe (or other transition-metal ion) hydrido species favors HER catalysis in a large number of cases, as Me−H are commonly reported as intermediates or active species in transition-metal-catalyzed H_2 production and oxidation.[1,61−68]

Therefore, we have studied Fe−H formation through an acid-assisted (AcOH) proton transfer from the cyanide in **1HHa** (Figure 6, light blue profile). This process occurs through **TS(1HHa→c)**, and its activation barrier is 17.4 kcal/mol, much lower than that obtained for the direct H_2 release from **1HHa**. The Fe ion involved in the proton migration is that coordinated by the cyanide. Indeed, no terminal hydride coordinated to the other Fe atom has been detected, except for a Fe−H−$C_{carbyne}$ bridging hydride, which, however, is 15.0 kcal/mol higher in energy with respect to **1HHa**.

The formation of Fe−H is concomitant with the shift of the carbene ligand from the Fe_2 bridging position to a terminal position at a single Fe.

1HHc easily and quickly isomerizes to the most stable Fe−H−Fe species (**1HHd**) (see Figure 6, light blue lines). Both **1HHc** and **1HHd** feature a protonated carbyne and an Fe hydride (which is t-H in the former and μ-H-Fe_2 in the latter). H_2 evolution from both species might occur through **TS(1HHc/d→1+H_2)**, which, however, was too energetically costly (activation barrier 37.6 kcal/mol starting from **1HHc**) (Figure 6, dotted light blue lines). The related transition state is associated with direct H_2 evolution without the formation of a (transient) Fe-H_2 σ complex. Indeed, structures with such a coordination mode were thermodynamically very unstable (higher than 26 kcal/mol vs ground state). The assistance of an acid molecule to form and release H_2 starting from both **1HHc** and **1HHd** has also been invoked. As already observed for **TS′(1HHa→1+H_2)**, the inclusion of an AcOH molecule as a proton shuttle in **TS′(1HHc/d→1+H_2)** (Figure 6, light blue lines) lowers the activation barrier, but not enough to make it compatible with a viable H_2 release.

1HHc can alternatively rearrange to the slightly less stable **1HHe**, through a low activation barrier (2.5 kcal/mol **TS(1HHa→c)**, Figure 6, orange profile). In **1HHe** the hydride is bridged between the Fe atom bound to CN^- and the C atom

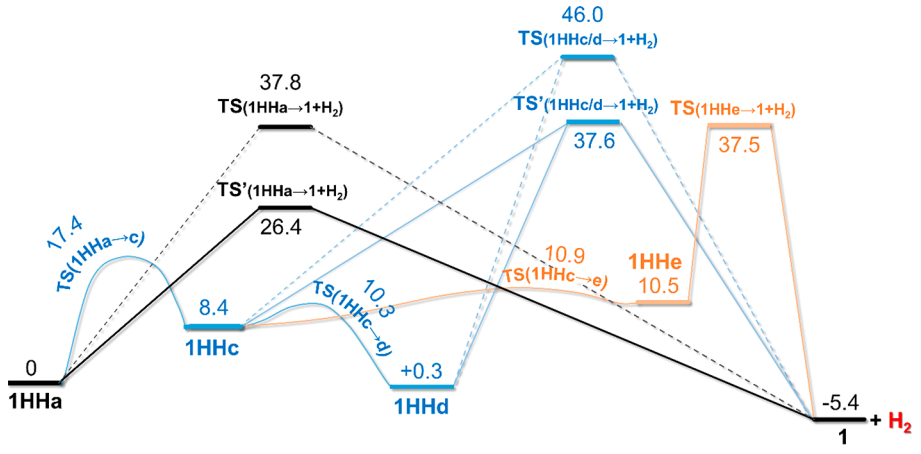

Figure 6. Global picture of the alternative pathways associated with H_2 production and release starting from **1HHa**. Energies (G) are given in kcal/mol. See Figure 7 for a visual inspection of structures related to the various pathways.

DOI: 10.1021/acs.inorgchem.7b01954
Inorg. Chem. 2017, 56, 13852−13864

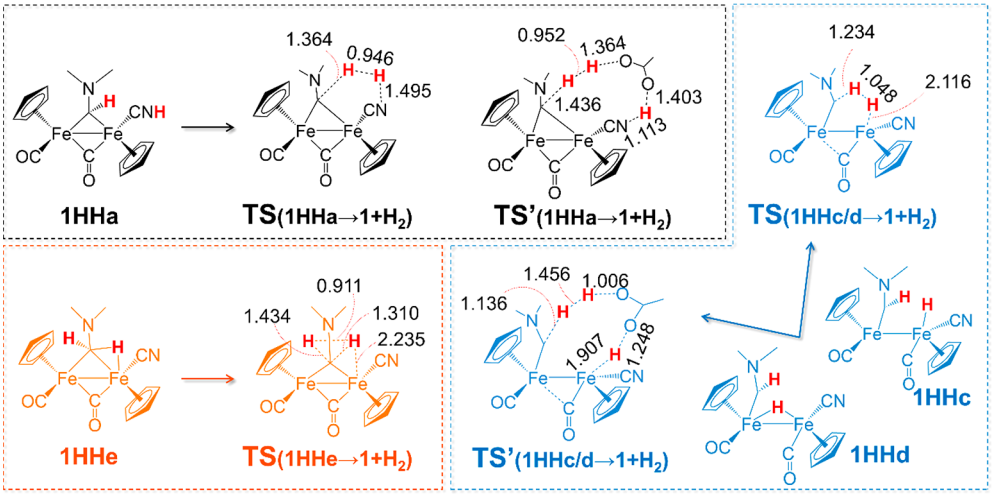

Figure 7. Structures of the most relevant **1HH** isomers and transition states involved in Figure 6. Distances are given in Å.

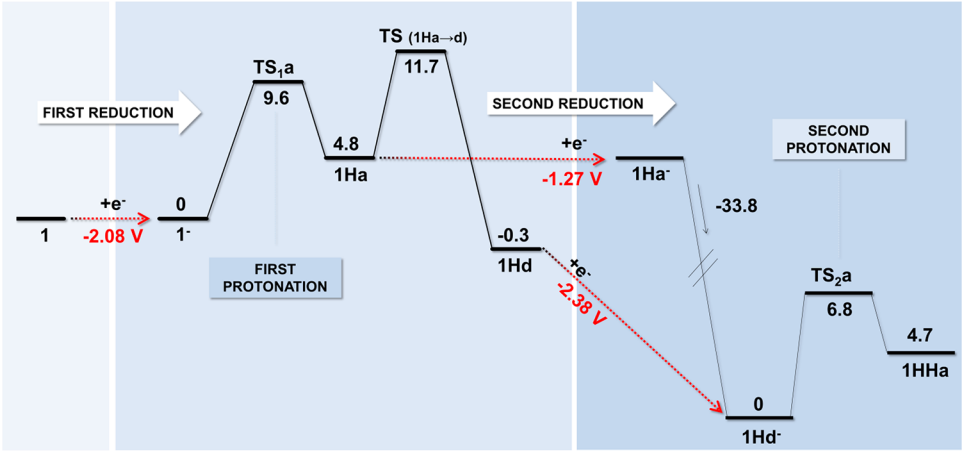

Figure 8. Summary of the lowest energy pathway associated with the formation of **1HHa**. Relative energies are given in kcal/mol and reduction potentials in V.

of μ-C(H)NMe$_2$. At this point H_2 release can occur through **TS′(1HHe→1+H$_2$)**, in which H_2 formation is almost completely assisted by the C atom of the aminocarbyne ligand (Figure 7, orange structures). However, this process involving **1HHe** formation and subsequent release of H_2 requires an overall barrier (37.5 kcal/mol) that is prohibitive for H_2 production.

Summary. The lowest energy pathway associated with the formation of the doubly reduced/doubly protonated **1HHa** is presented in Figure 8, and it can be summarized as follows: (i) first one-electron reduction, (ii) first protonation, occurring at cyanide, (iii) second one-electron reduction and migration of the proton from the cyanide to the aminocarbyne carbon atom, and (iv) second protonation, occurring at cyanide. The optimized structure of the lowest energy TS for H_2 release (**TS(1HHa→1+H$_2$)**) is presented in Figure 9.

The DFT mechanism herein proposed for HER emphasizes the general message that metal complexes have often the tendency to be first protonated at a site *which is not the metal itself,* but a weakly basic functional group in the metal coordination sphere: e.g., CN^- in **1**. In electron-rich dithiolates such a role is played by sulfur atoms, as demonstrated by Zaffaroni et al.[69] In that and also other biomimetic dithiolates, the accepted picture for the HER entails a subsequent proton

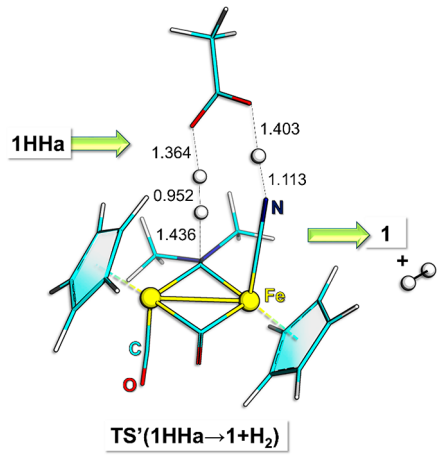

Figure 9. Representation of the H_2 release process from **1HHa**. The optimized structure of the involved transition state is also presented. Displayed distances are given in Å.

relay occurring from the weak base to one metal center that forms either terminal or bridging metal hydrides, prompted for H_2 formation, as evidenced by Gloaguen and Rauchfuss.[42] Remarkably, however, in the present case study the proton

DOI: 10.1021/acs.inorgchem.7b01954
Inorg. Chem. 2017, 56, 13852−13864

Scheme 2. Energetically Viable Pathway for Proton Reduction Mediated by 1

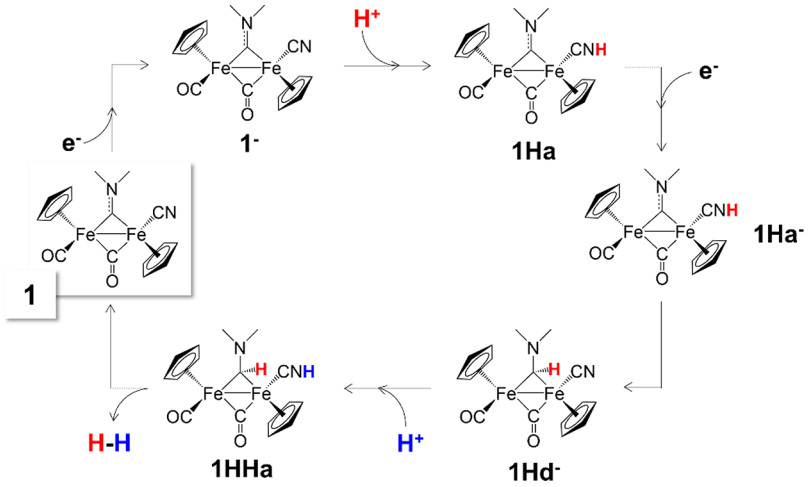

relay from the cyanide is directed to the amino-carbyne ligand rather than to Fe.

The overall mechanism, summarized in Scheme 2, provides a picture compatible with a completely "ligand based" electrocatalysis, in which a clear noninnocent behavior of ligands involves both redox and acid−base processes underlying the HER. The ligand-based catalysis performed by **1** is in perfect agreement with its saturated valence 36e $(Fe^{I})_2$ core, thus working as a collecting point of reactants.[70] Nonetheless, in addition to providing a topological function of appropriately disposing the proximity of the reaction centers, Fe atoms take part in catalysis by tuning the ligand reactivity to favor the HER. Actually, (i) the Fe ions moderately drain electron density from cyanide (thus favoring proton trafficking between ligands, vide infra) and (ii) help to localize the carbyne LUMO onto C, which is the exact catalytic site of reduction (vide infra). Apfel, Vos, and Weigand reported that the L σ-donor properties in monosubstituted $\{Fe_2(CO)_5[\mu\text{-}(CH_2S)_2Si(R_2)]\text{-}L\}$ (L = CN^-, PPh_3) were not fully consistent with the observed electrochemical behavior of such derivatives, leading them to postulate that elusive HOMO−LUMO variations could have been operating.[71]

Overall, the ligand-based reactivity of transition-metal compounds is very well documented in the literature as well as the modifications brought about by ligand coordination to metal centers.[70]

Role of Cyanide. The DFT dissection of the catalytic mechanism presented above suggests that CN^- ligand provides, on the one hand, a kinetically accessible protonation site, thus favoring a crucial step of the catalytic HER. On the other hand, CN^- is not thermodynamically so basic as to prevent H^+ from being subsequently conveyed to carbyne. The proton relay exerted by CN^- is interesting since it is unusual in typical diiron clusters modeling [Fe−Fe]-H_2ases, although two cyanides are present in the enzyme cofactor. Indeed, in the Fe_2 core of the H cluster, the role of proton relay from the outer environment to metal is not played by coordinated CN^- ions (anchored to the protein matrix through noncovalent interactions) but by the central nitrogen of the aza-dithiolate linker.

In the context of synthetic mimicry of H_2ase, one of the problems arising from the incorporation of cyanides in the Fe_2S_2 scaffold is (in some cases) their overly large proton affinity.[72,73] Actually, the NBO analysis (data not shown) of the atomic partial charges of the electrocatalytically inactive[72b] $\{Fe_2[\mu\text{-}S_2(CH_2)_3](CN)_2(CO)_4\}^{2-}$ shows a ca. 2-fold increase of cyanide negative charge upon reduction in comparison to that we have observed for reduction of **1** (see Figure 10).

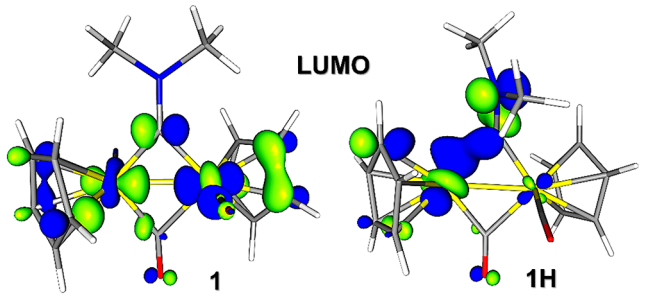

Δq NBO	1⁻ - 1	1H⁻ - 1H
μ-$CNMe_2$	-0.17	-0.20
CN^-	-0.09	-0.10
Fe's	0.06 0.06	0.02 0.01

ΔE = $E_{(CNH^+)} - E_{(\mu\text{-}C(H^+)NMe_2)}$	
$1H^+$	31.9
1H	-8.3
$1H^-$	-33.8

Figure 10. (top) LUMO shapes of most stable isomers of **1** and **1H**. (bottom left) NBO charge variations upon first and second reductive events. (bottom right) relative energies (in kcal/mol) of isomers featuring protonated cyanide (CNH^+) vs protonated carbyne (C-$(H^+)N(Me)_2$) as a function of the redox state.

However, Rauchfuss et al. reported that replacing a CO with a PMe_3 ligand is effective to observe catalysis of proton reduction.[42] In that particular case, the chemical ingredients necessary to HER were (i) a single cyanide, (ii) at least another σ donor (the mono-CN complex did not show HER, probably because of an overly large stability of $Fe_2(CNH)$ species), and (iii) the Fe−Fe bond presence (becoming the hydridic site once the complex underwent the second protonation).

Differently from $Fe_2(\mu\text{-pdt})(CN)(CO)_4(PMe_3)$ (and probably all other H_2ase mimics), CN^- in **1** does not increase electron density at the Fe−Fe core, as demonstrated by the inspection of atomic partial charges. This is also consistent with the proposed "ligand based" electrocatalytic mechanism. The metal plays a role by moderately withdrawing electron density from CN^- that, otherwise, would be too basic (NBO partial charges: C(−0.3)−N(−0.7) vs Fe−C(−0.1)−N(−0.2)) to subsequently release H^+ to the carbyne. The simultaneous presence of both CN^- and carbyne ligands turns out thus to be

DOI: 10.1021/acs.inorgchem.7b01954
Inorg. Chem. 2017, 56, 13852−13864

essential because the proton affinity of the former is properly balanced to allow the proton release to the latter.

After the second reduction of the ECEC scheme, CN^- can be easily protonated and plays its second, crucial role in the entire catalytic cycle. In fact, it is directly involved in the H_2 formation process, acting as a proton source in the $H^+ + H^- \rightarrow H_2$ process (through the transient assistance of a AcOH molecule). All this makes **1** suited for HER catalysis, although its performance could possibly be improved (vide infra).

These observations are sufficient to rationalize the inactivity of **2** (that differs from **1** for the CN^- replacement by CO) toward the HER. The subtle role played by CN^- in the electrocatalyis of HER mediated by **1** is demonstrated by the experimental observation that replacing CN^- by another negatively charged ligand (N_3^-) completely abolished HER detection. The full characterization of the azido-Fe derivative will be subject of a forthcoming investigation. However, preliminary DFT results suggest that the HN_3 is readily expelled by the Fe_2 scaffold (the activation barrier associated with Fe−(HN_3) bond breaking is 2.0 kcal/mol, data not shown). Thus, the inactivity of this species is fully justified and the double role played by CN^- is further confirmed.

Role of Carbyne. The relative stability between the isomer featuring a protonated cyanide and the isomer with protonated carbyne is completely inverted upon double reduction, as arises from $\mathbf{1H}^+$, **1H**, and $\mathbf{1H}^-$ thermodynamic speciation (see Figure 2 and Figure 10, bottom right).

The increasing stability of isomers with protonated carbyne upon reduction is due to a significant increase in the electron density on such a ligand. Indeed, when the two reductive steps involved in catalysis, $\mathbf{1} \rightarrow \mathbf{1}^-$ and $\mathbf{1H} \rightarrow \mathbf{1H}^-$ (focusing on the portions of the molecule directly involved in the mechanism), are considered, the variation of NBO charge at the carbyne ligand is 2-fold that at the cyanide, while the charge on metal centers is almost the same independently from the redox state of the system. In addition, the LUMO of **1** has a significant component of the carbyne C atom, through one of its p orbitals. The distribution of the LUMO on the carbyne ligand becomes even more evident upon first protonation/reduction, in **1H**. As a result, on going from **1** to $\mathbf{1H}^-$ the carbyne ligand stores electron density and one proton to form a carbene with tetrahedral geometry and one C−H bond. The HER-type activity of this bond, however, is not high, as suggested by the activation barrier (26.4 kcal/mol) associated with the H_2 release. The synthetic versatility of the carbyne ligand could be easily exploited to design carbon-based groups with more reactive C−H bonds. In this context, $-CN(Me)_2$ has proved able to store negative charge during turnover, in analogy to a number of cases in which ligands can act as electron reservoirs, modulating or even enhancing the redox properties of first-row transition-metal-containing catalysts.[74−76]

CONCLUDING REMARKS

A suggestion emerging from the present study to develop better-performing variants of **1** concerns the design of a more efficient heterocoupling of hydride and proton. Synthetic modeling efforts should be made with the aim of achieving a closer H^-/H^+ spacing that could allow elimination of the acid dependence. In fact, an intramolecular (or direct) proton shuttling process away from CN^- to H^- is expected to occur more quickly and efficiently in comparison to an intermolecular (or mediated) process. Also, the incorporation of a highly versatile ligand such as carbyne in the Fe_2 scaffold affords the opportunity to further explore the effects related to the switch from metal-based to ligand-based processes. This switch can provide practical advantages that go beyond the scope of the HER. Among the large number of examples of ligand-based reactivity (with special focus on catalysis), the following are worth mentioning: (i) CO_2 reduction to CO on Fe,[76] (ii) CO_2 reduction to CO on NbN,[77] (iii) alkyne methatesis on Mo(VI),[78] and (iv) C−H activation through C−N formation mediated by Co and Ru dinitrosyl complexes.[79] In another example not directly related to catalysis, but of high technological relevance, NiS_4 complexes are reported to selectively and reversibly bind light olefins through S atoms.[80] Avoidance of metal binding implies high tolerance to poisoning by H_2, CO, H_2S, and C_2H_2 gases, thus affording a robust, profitable approach to separate ethylene and propylene from industrial streams.

By specifically refocusing on the electrochemical HER whose catalysis occurs according to ligand-based mechanisms, very recent examples have been reported for Ni and Fe complexes. Among others, it is worth citing the investigations on NiS_4-based (of outstanding interest as resembling the Ni environment in the [NiFe]-H_2ase) catalysts of the HER by Artero and Mitsopoulou[81] and those on NiS_4[82] and on $Fe_2(\mu\text{-}S)_2$[83] by the Yamauchi and Sakai groups.

In conclusion and to the best of our knowledge, **1** represents the first example of an electrocatalytically HER-competent catalyst that simultaneously (i) is based on a nonprecious dimetallic core (Fe_2), (ii) is dithiolate-free, and (iii) works with no (even transient) formation of Me-H intermediates. μ-Carbyne and t-CN metal ligands provides all acid−base and redox requisites necessary for the heterocoupling of hydrides and protons.

ASSOCIATED CONTENT

Supporting Information

The Supporting Information is available free of charge on the ACS Publications website at DOI: 10.1021/acs.inorgchem.7b01954.

Optimized structures of **1** and $\mathbf{2}^+$ isomers, with an extended geometrical analysis at different levels of theory (BP86, B3LYP, M06), relative energies between cis and trans isomers, at each redox state, together with the main geometrical parameters of singly and doubly reduced species, NBO charge variations upon first and second reductions, LUMO shapes, and Mulliken atomic populations of both **1** and $\mathbf{2}^+$, overall scheme summarizing all the pinpointed pathways for H_2 evolution (alternative to Scheme 2), activation barriers, obtained at the B3LYP/TZVP level, associated with all the characterized transition states, thermodynamic speciation of each protonated and/or reduced intermediate involved in catalysis, and coordinates of the main optimized stationary points (PDF)

AUTHOR INFORMATION

Corresponding Authors

*E-mail for V.Z.: valerio.zanotti@unibo.it.

*E-mail for G.Z.: giuseppe.zampella@unimib.it.

ORCID

Luca Bertini: 0000-0003-3402-0846

Rita Mazzoni: 0000-0002-8926-9203

Valerio Zanotti: 0000-0003-4190-7218

DOI: 10.1021/acs.inorgchem.7b01954
Inorg. Chem. 2017, 56, 13852−13864

Giuseppe Zampella: 0000-0003-0517-6016

Notes

The authors declare no competing financial interest.

■ ACKNOWLEDGMENTS

We are very grateful to Prof. Roberto Della Pergola for fruitful discussions on the topic treated in the present contribution and to Dr. Paolo Saponaro for helping in the preparation of some materials.We thank the Ministero dell'Università e della Ricerca Scientifica e Tecnologica (MIUR) for financial support (PRIN 2015, 20154X9ATP_003).

■ REFERENCES

(1) Schilter, D.; Camara, J. M.; Huynh, M. T.; Hammes-Schiffer, S.; Rauchfuss, T. B. Hydrogenase enzymes and their synthetic models: the role of metal hydrides. *Chem. Rev.* **2016**, *116*, 8693−8749.

(2) Gloaguen, F. Electrochemistry of simple organometallic models of iron−iron hydrogenases in organic solvent and water. *Inorg. Chem.* **2016**, *55*, 390−398.

(3) Bullock, R. M. *Catalysis Without Precious Metals*; Wiley-VCH: Weinheim, Germany, 2010.

(4) Li, Y.; Rauchfuss, T. B. Synthesis of diiron(I) dithiolato carbonyl complexes. *Chem. Rev.* **2016**, *116*, 7043−7077.

(5) Capon, J. F.; Gloaguen, F.; Pétillon, F. Y.; Schollhammer, P.; Talarmin, J. Electron and proton transfers at diiron dithiolate sites relevant to the catalysis of proton reduction by the [FeFe]-hydrogenases. *Coord. Chem. Rev.* **2009**, *253*, 1476−1494.

(6) Mejia-Rodriguez, R.; Chong, D. S.; Reibenspies, J. H.; Soriaga, M. P.; Darensbourg, M. Y. The hydrophilic phosphatriazaadamantane ligand in the development of H_2 production electrocatalysts: iron hydrogenase model complexes. *J. Am. Chem. Soc.* **2004**, *126*, 12004−12014.

(7) Cheah, M. H.; Tard, C.; Borg, S. J.; Liu, X.; Ibrahim, S. K.; Pickett, C. J.; Best, S. P. Modeling [Fe−Fe] hydrogenase: evidence for bridging carbonyl and distal iron coordination vacancy in an electrocatalytically competent proton reduction by an iron thiolate assembly that operates through Fe(0)−Fe(II) levels. *J. Am. Chem. Soc.* **2007**, *129*, 11085−11092.

(8) Harb, M. K.; Apfel, U. P.; Kubel, J.; Gorls, H.; Felton, G. A. N.; Sakamoto, T.; Evans, D. H.; Glass, R. S.; Lichtenberger, D. L.; El-Khateeb, M.; Weigand, W. Preparation and characterization of homologous diiron dithiolato, diselenato, and ditellurato complexes: [FeFe]-hydrogenase models. *Organometallics* **2009**, *28*, 6666−6675.

(9) Mazzoni, R.; Gabiccini, A.; Cesari, C.; Zanotti, V.; Gualandi, I.; Tonelli, D. Diiron complexes bearing bridging hydrocarbyl ligands as electrocatalysts for proton reduction. *Organometallics* **2015**, *34*, 3228−3235.

(10) Yang, D.; Li, Y.; Wang, B.; Zhao, X.; Su, L.; Chen, S.; Tong, P.; Luo, Y.; Qu, J. Synthesis and electrocatalytic property of diiron hydride complexes derived from a thiolate-bridged diiron complex. *Inorg. Chem.* **2015**, *54*, 10243−10249.

(11) Nicolet, Y.; de Lacey, A. L.; Vernede, X.; Fernandez, V. M.; Hatchikian, E. C.; Fontecilla-Camps, J. C. Crystallographic and FTIR spectroscopic evidence of changes in Fe coordination upon reduction of the active site of the Fe-only hydrogenase from Desulfovibrio desulfuricans. *J. Am. Chem. Soc.* **2001**, *123*, 1596−1601.

(12) Berggren, G.; Adamska, A.; Lambertz, C.; Simmons, T. R.; Esselborn, J.; Atta, M.; Gambarelli, S.; Mouesca, J. M.; Reijerse, E.; Lubitz, W.; Happe, T.; Artero, V.; Fontecave, M. Biomimetic assembly and activation of [FeFe]-hydrogenases. *Nature* **2013**, *499*, 66−69.

(13) Tard, C.; Pickett, C. J. Structural and functional analogues of the active sites of the [Fe]-, [NiFe]-, and [FeFe]-hydrogenases. *Chem. Rev.* **2009**, *109*, 2245−2274.

(14) Wang, N.; Wang, M.; Liu, J.; Jin, K.; Chen, L.; Sun, L. Preparation, facile deprotonation, and rapid H/D exchange of the mu-hydride diiron model complexes of the [FeFe]-hydrogenase containing a pendant amine in a chelating diphosphine ligand. *Inorg. Chem.* **2009**, *48*, 11551−11558.

(15) Ezzaher, S.; Capon, J. F.; Gloaguen, F.; Petillon, F. Y.; Schollhammer, P.; Talarmin, J.; Kervarec, N. Influence of a pendant amine in the second coordination sphere on proton transfer at a dissymmetrically disubstituted diiron system related to the $[2Fe]_H$ subsite of $[FeFe]H_2$ase. *Inorg. Chem.* **2009**, *48*, 2−4.

(16) Wang, Y. W.; Li, Z. M.; Zeng, X. H.; Wang, X. F.; Zhan, C. X.; Liu, Y. Q.; Zeng, X. R.; Luo, Q. Y.; Liu, X. M. Synthesis and characterisation of three diiron tetracarbonyl complexes related to the diiron centre of [FeFe]-hydrogenase and their protonating, electrochemical investigations. *New J. Chem.* **2009**, *33*, 1780−1789.

(17) Olsen, M. T.; Rauchfuss, T. B.; Wilson, S. R. Role of the azadithiolate cofactor in models for [FeFe]-hydrogenase: novel structures and catalytic implications. *J. Am. Chem. Soc.* **2010**, *132*, 17733−17740.

(18) Tschierlei, S.; Ott, S.; Lomoth, R. Spectroscopically characterized intermediates of catalytic H_2 formation by [FeFe] hydrogenase models. *Energy Environ. Sci.* **2011**, *4*, 2340−2352.

(19) Zheng, D. H.; Wang, N.; Wang, M.; Ding, S. D.; Ma, C. B.; Darensbourg, M. Y.; Hall, M. B.; Sun, L. C. Intramolecular iron-mediated C−H bond heterolysis with an assist of pendant base in a [FeFe]-hydrogenase model. *J. Am. Chem. Soc.* **2014**, *136*, 16817−16823.

(20) Arrigoni, F.; Mohamed Bouh, S.; De Gioia, L.; Elleouet, C.; Pétillon, F. Y.; Schollhammer, P.; Zampella, G. Influence of the dithiolate bridge on the oxidative processes of diiron models related to the active site of [FeFe] hydrogenases. *Chem. - Eur. J.* **2017**, *23*, 4364−4372.

(21) Ahlrichs, R.; Bar, M.; Haser, M.; Horn, H.; Kolmel, C.; Ahlrichs, R.; Bär, M.; Häser, M.; Horn, H.; Kölmel, C. Electronic structure calculations on workstation computers: The program system Turbomole. *Chem. Phys. Lett.* **1989**, *162*, 165−169.

(22) (a) Becke, A. D. Density-functional exchange-energy approximation with correct asymptotic behavior. *Phys. Rev. A: At., Mol., Opt. Phys.* **1988**, *38*, 3098−3100. (b) Perdew, J. P. Density-functional approximation for the correlation energy of the inhomogeneous electron gas. *Phys. Rev. B: Condens. Matter Mater. Phys.* **1986**, *33*, 8822−8824.

(23) Schafer, A.; Huber, C.; Ahlrichs, R. Fully optimized contracted Gaussian basis sets of triple zeta valence quality for atoms Li to Kr. *J. Chem. Phys.* **1994**, *100*, 5829−5835.

(24) Zampella, G.; Bruschi, M.; Fantucci, P.; Razavet, M.; Pickett, C. J.; De Gioia, L. Dissecting the intimate mechanism of cyanation of {2Fe3S} complexes related to the active site of all-iron hydrogenases by DFT analysis of energetics, transition states, intermediates and products in the carbonyl substitution pathway. *Chem. - Eur. J.* **2005**, *11*, 509−533.

(25) Tard, C.; Liu, X.; Ibrahim, S. K.; Bruschi, M.; De Gioia, L.; Davies, S. C.; Yang, X.; Wang, L.-S.; Sawers, G.; Pickett, C. J. Synthesis of the H-cluster framework of iron-only hydrogenase. *Nature* **2005**, *433*, 610−613.

(26) Boyke, C. A.; van der Vlugt, J. I.; Rauchfuss, T. B.; Wilson, S. R.; Zampella, G.; De Gioia, L. Diferrous cyanides as models for the Fe-only hydrogenases. *J. Am. Chem. Soc.* **2005**, *127*, 11010−11018.

(27) Zampella, G.; Bruschi, M.; Fantucci, P.; De Gioia, L. DFT Investigation of H_2 activation by $[M(NHPnPr_3)('S3')]$ (M = Ni, Pd). Insight into key factors relevant to the design of hydrogenase functional models. *J. Am. Chem. Soc.* **2005**, *127*, 13180−13189.

(28) Zampella, G.; Fantucci, P.; De Gioia, L. Unveiling how stereoelectronic factors affect kinetics and thermodynamics of protonation regiochemistry in [FeFe] hydrogenase synthetic models: a DFT investigation. *J. Am. Chem. Soc.* **2009**, *131*, 10909−10917.

(29) Chouffai, D.; Zampella, G.; Capon, J.-F.; De Gioia, L.; Le Goff, A.; Petillon, F. Y.; Schollhammer, P.; Talarmin, J. Electrochemical and theoretical studies of the impact of the chelating ligand on the reactivity of $[Fe_2(CO)_4(\kappa^2\text{-LL})(\mu\text{-pdt})]$ complexes with different substrates (LL = IMe-CH_2-IMe, dppe; IMe= 1-Methylimidazol-2-ylidene). *Organometallics* **2012**, *31*, 1082−1091.

DOI: 10.1021/acs.inorgchem.7b01954
Inorg. Chem. 2017, 56, 13852−13864

(30) (a) Lee, C.; Yang, W.; Parr, R. G. Development of the Colle-Salvetti correlation-energy formula into a functional of the electron density. *Phys. Rev. B: Condens. Matter Mater. Phys.* **1988**, *37*, 785−789. (b) Becke, A. D. Density-functional thermochemistry. III. The role of exact exchange. *J. Chem. Phys.* **1993**, *98*, 5648−5652.
(31) Roy, L. E.; Batista, E. R.; Hay, P. J. Theoretical studies on the redox potentials of Fe dinuclear complexes as models for hydrogenase. *Inorg. Chem.* **2008**, *47*, 9228−9237.
(32) Zhao, Y.; Truhlar, D. G. The M06 suite of density functionals for main group thermochemistry, thermochemical kinetics, noncovalent interactions, excited states, and transition elements: two new functionals and systematic testing of four M06-class functionals and 12 other functionals. *Theor. Chem. Acc.* **2008**, *120*, 215−241.
(33) (a) Klamt, A. Conductor-like screening model for real solvents: a new approach to the quantitative calculation of solvation phenomena. *J. Phys. Chem.* **1995**, *99*, 2224−2235. (b) Klamt, A. Calculation of UV/Vis spectra in solution. *J. Phys. Chem.* **1996**, *100*, 3349−3353.
(34) Jensen, F. *Introduction to Computational Chemistry*; Wiley: Chichester, England, 2007.
(35) *WIREs Comput. Mol. Sci.* **2012**, *2*: 1−42 10.1002/wcms.51.
(36) Filippi, G.; Arrigoni, F.; Bertini, L.; De Gioia, L.; Zampella, G. DFT dissection of the reduction step in H_2 catalytic production by [FeFe]-hydrogenase-inspired models: can the bridging hydride become more reactive than the terminal isomer? *Inorg. Chem.* **2015**, *54*, 9529−9542.
(37) Albano, V. G.; Busetto, L.; Marchetti, F.; Monari, M.; Zanotti, V. Acetonitrile activation in di-iron μ-carbyne complexes: synthesis and structure of the cyanomethyl complex [Fe2(μ-CNMe2)(μ-CO)(CO)-(CH2CN)(Cp)2]. *J. Organomet. Chem.* **2002**, *649*, 64−69.
(38) Busetto, L.; Marchetti, F.; Zacchini, S.; Zanotti, V. Diiron and diruthenium aminocarbyne complexes containing pseudohalides: stereochemistry and reactivity. *Inorg. Chim. Acta* **2005**, *358*, 1204−1216.
(39) Borg, S. J.; Behrsing, T.; Best, S. P.; Razavet, M.; Liu, X.; Pickett, C. J. Electron transfer at a dithiolate-bridged diiron assembly: electrocatalytic hydrogen evolution. *J. Am. Chem. Soc.* **2004**, *126*, 16988−16999.
(40) Bourrez, M.; Steinmetz, R.; Gloaguen, F. Mechanistic insights into the catalysis of electrochemical proton reduction by a diiron azadithiolate complex. *Inorg. Chem.* **2014**, *53*, 10667−10673.
(41) Surawatanawong, P.; Tye, J. W.; Darensbourg, M. Y.; Hall, M. B. Mechanism of electrocatalytic hydrogen production by a di-iron model of iron−iron hydrogenase: A density functional theory study of proton dissociation constants and electrode reduction potentials. *Dalton Trans.* **2010**, *39*, 3093−3104.
(42) Gloaguen, F.; Lawrence, J. D.; Rauchfuss, T. B. Biomimetic hydrogen evolution catalyzed by an iron carbonyl thiolate. *J. Am. Chem. Soc.* **2001**, *123*, 9476−9477.
(43) Chong, D.; Georgakaki, I. P.; Mejia-Rodriguez, R.; Sanabria-Chinchilla, J.; Soriaga, M. P.; Darensbourg, M. Y. Electrocatalysis of hydrogen production by active site analogues of the iron hydrogenase enzyme: structure/function relationships. *Dalton Trans.* **2003**, 4158−4163.
(44) Felton, G. A. N.; Vannucci, A. K.; Chen, J.; Lockett, L. T.; Okumura, N.; Petro, B. J.; Zakai, U. I.; Evans, D. H.; Glass, R. S.; Lichtenberger, D. L. Hydrogen generation from weak acids: electrochemical and computational studies of a diiron hydrogenase mimic. *J. Am. Chem. Soc.* **2007**, *129*, 12521−12530.
(45) Almazahreh, L. R.; Apfel, U. P.; Imhof, W.; Rudolph, M.; Görls, H.; Talarmin, J.; Schollhammer, P.; El-khateeb, M.; Weigand, W. A novel [FeFe] hydrogenase model with a $(SCH_2)_2P{=}O$ moiety. *Organometallics* **2013**, *32*, 4523−4530.
(46) Cox, M. G.; Dowling, C.; Manning, A. R.; Mcardle, P.; Cunningham, D. A reinvestigation of the reaction of $[Fe_2(\eta\text{-}C_5H_5)_2(CO)_{4-n}(CNR)_n]$ (n = 1 or 2) with strong alkylating agents. *J. Organomet. Chem.* **1992**, *438*, 143−158.
(47) Boss, K.; Cox, M. G.; Dowling, C.; Manning, A. R. The reactions of cis-$[Fe_2(\eta\text{-}C_5H_5)_2(CO)_2(\mu\text{-}CNMe_2)_2][SO_3CF_3]_2$ and related compounds with nucleophiles. *J. Organomet. Chem.* **2000**, *612*, 18−35.
(48) Pombeiro, A. J. L. Coordination chemistry of CNH, the simplest isocyanide. *Inorg. Chem. Commun.* **2001**, *4*, 585−597.
(49) Bullock, R. M.; Appel, A. M.; Helm, M. L. Production of hydrogen by electrocatalysis: making the H−H bond by combining protons and hydrides. *Chem. Commun.* **2014**, *50*, 3125−3143.
(50) Raugei, S.; Helm, M. L.; Hammes-Schiffer, S.; Appel, A. M.; O'Hagan, M.; Wiedner, E. S.; Bullock, R. M. Experimental and computational mechanistic studies guiding the rational design of molecular electrocatalysts for production and oxidation of hydrogen. *Inorg. Chem.* **2016**, *55*, 445−460.
(51) Barton, B. E.; Zampella, G.; Justice, A. K.; De Gioia, L.; Rauchfuss, T. B.; Wilson, S. R. Isomerization of the hydride complexes $[HFe_2(SR)_2(PR_3)_x(CO)_{6-x}]^+$ (x = 2, 3, 4) relevant to the active site models for the [FeFe]-hydrogenases. *Dalton Trans* **2010**, *39*, 3011−3019.
(52) Zampella, G.; Fantucci, P.; De Gioia, L. DFT characterization of the reaction pathways for terminal- to μ-hydride isomerisation in synthetic models of the [FeFe]-hydrogenase active site. *Chem. Commun.* **2009**, *46*, 8824−8826.
(53) Barton, B. E.; Rauchfuss, T. B. Terminal hydride in [FeFe]-hydrogenase model has lower potential for H_2 production than the isomeric bridging hydride. *Inorg. Chem.* **2008**, *47*, 2261−2263.
(54) van der Vlugt, J. I.; Rauchfuss, T. B.; Whaley, C. M.; Wilson, S. R. Characterization of a diferrous terminal hydride mechanistically relevant to the Fe-only hydrogenases. *J. Am. Chem. Soc.* **2005**, *127*, 16012−16013.
(55) Yu, X.; Tung, C.; Wang, W.; Huynh, M. T.; Gray, D. L.; Hammes-Schiffer, S.; Rauchfuss, T. B. Interplay between terminal and bridging diiron hydrides in neutral and oxidized states. *Organometallics* **2017**, *36*, 2245−2253.
(56) Albano, V. G.; Busetto, L.; Monari, M.; Zanotti, V. Reactions of acetonitrile di-iron μ-aminocarbyne complexes; synthesis and structure of $[Fe_2(\mu\text{-}CNMe_2)(\mu\text{-}H)(CO)_2(Cp)_2]$. *J. Organomet. Chem.* **2000**, *606*, 163−168.
(57) Zanotti, V.; Bordoni, S.; Busetto, L.; Carlucci, L.; Palazzi, A.; Serra, R.; Albano, V. G.; Monari, M.; Prestopino, F.; Laschi, F.; Zanello, P. Diiron aminoalkylidene complexes. *Organometallics* **1995**, *14*, 5232−5241.
(58) Busetto, L.; Carlucci, L.; Zanotti, V.; Albano, V. G.; Braga, D. Synthesis, reactions, and X-ray structures of the functionalized isocyanide complexes $[Fe_2\{\mu\text{-}CNC(O)SR\}(\mu\text{-}CO)(CO)_2(cp)_2]$(cp = $\eta\text{-}C_5H_5$, R = Me or Et) and of their carbyne and carbene derivatives. *J. Chem. Soc., Dalton Trans.* **1990**, 243−250.
(59) (a) Simmons, T. R.; Berggren, G.; Bacchi, M.; Fontecave, M.; Artero, V. Mimicking hydrogenases: From biomimetics to artificial enzymes. *Coord. Chem. Rev.* **2014**, *270*−*271*, 127−150. (b) Sommer, C.; Adamska-Venkatesh, A.; Pawlak, K.; Birrel, J. A.; Rudiger, O.; Reijerse, E. J.; Lubitz, W. Proton coupled electronic rearrangement within the H-Cluster as an essential step in the catalytic cycle of [FeFe]-hydrogenases. *J. Am. Chem. Soc.* **2017**, *139*, 1440−1443.
(60) Zhou, X.; Barton, B. E.; Chambers, G. M.; Rauchfuss, T. B.; Arrigoni, F.; Zampella, G. Preparation and protonation of $Fe_2(pdt)(CNR)_6$, electron-rich analogues of $Fe_2(pdt)(CO)_6$. *Inorg. Chem.* **2016**, *55*, 3401−3412.
(61) Rauchfuss, T. B. Diiron azadithiolates as models for the [FeFe]-hydrogenase active site and paradigm for the role of the second coordination sphere. *Acc. Chem. Res.* **2015**, *48*, 2107−2116.
(62) Wilson, A. D.; Newell, R. H.; McNevin, M. J.; Muckerman, J. T.; DuBois, M. R.; DuBois, D. L. Hydrogen oxidation and production using nickel-based molecular catalysts with positioned proton relays. *J. Am. Chem. Soc.* **2006**, *128*, 358−366.
(63) McKone, J. R.; Marinescu, S. C.; Brunschwig, B. S.; Winkler, J. R.; Gray, H. B. Earth-abundant hydrogen evolution electrocatalysts. *Chem. Sci.* **2014**, *5*, 865−878.
(64) Darmon, J. M.; Raugei, S.; Liu, T.; Hulley, E. B.; Weiss, C. J.; Bullock, R. M.; Helm, M. L. Iron complexes for the electrocatalytic

DOI: 10.1021/acs.inorgchem.7b01954
Inorg. Chem. 2017, 56, 13852−13864

oxidation of hydrogen: tuning primary and secondary coordination spheres. *ACS Catal.* **2014**, *4*, 1246−1260.
(65) Liu, T.; Liao, Q.; O'Hagan, M.; Hulley, E. B.; DuBois, D. L.; Bullock, R. M. Iron complexes bearing diphosphine ligands with positioned pendant amines as electrocatalysts for the oxidation of H_2. *Organometallics* **2015**, *34*, 2747−2764.
(66) Darmon, J. M.; Kumar, N.; Hulley, E. B.; Weiss, C. J.; Raugei, S.; Bullock, R. M.; Helm, M. L. Increasing the rate of hydrogen oxidation without increasing the overpotential: a bio-inspired iron molecular electrocatalyst with an outer coordination sphere proton relay. *Chem. Sci.* **2015**, *6*, 2737−2745.
(67) Connelly Robinson, S. J.; Heinekey, D. M. Hydride & dihydrogen complexes of earth abundant metals: structure, reactivity, and applications to catalysis. *Chem. Commun.* **2017**, *53*, 669−676.
(68) Brazzolotto, D.; Gennari, M.; Queyriaux, N.; Simmons, T. R.; Pécaut, J.; Demeshko, S.; Meyer, F.; Orio, M.; Artero, V.; Duboc, C. Nickel centred H^+ reduction catalysis in a model of [NiFe] Hydrogenase. *Nat. Chem.* **2016**, *8*, 1054−1060.
(69) Zaffaroni, R.; Rauchfuss, T. B.; Gray, D. L.; De Gioia, L.; Zampella, G. Terminal vs bridging hydrides of diiron dithiolates: protonation of Fe_2(dithiolate)$(CO)_2(PMe_3)_4$. *J. Am. Chem. Soc.* **2012**, *134*, 19260−19269.
(70) Wilkins, R. G. *Kinetics and Mechanism of Reactions of Transition Metal Complexes*, 2nd ed.; VCH Publishers: New York, 1991; Chapter 6.
(71) Apfel, U. P.; Halpin, Y.; Gorls, H.; Vos, J. G.; Weigand, W. Influence of the introduction of cyanido and phosphane ligands in multifunctionalized (mercaptomethyl)silane [FeFe] hydrogenase model systems. *Eur. J. Inorg. Chem.* **2011**, *2011*, 581−588.
(72) (a) Le Cloirec, A.; Best, S. P.; Borg, S.; Davies, S. C.; Evans, D. J.; Hughes, D. L.; Pickett, C. J. A di-iron dithiolate possessing structural elements of the carbonyl/cyanide sub-site of the H-centre of Fe-only hydrogenase. *Chem. Commun.* **1999**, 2285−2286. (b) Schmidt, M.; Contakes, S. M.; Rauchfuss, T. B. First generation analogues of the binuclear site in the Fe-only hydrogenases: $Fe_2(\mu\text{-SR})_2(CO)_4(CN)_2^{2-}$. *J. Am. Chem. Soc.* **1999**, *121*, 9736−9737.
(73) Lyon, E. J.; Georgakaki, I. P.; Reibenspies, J. H.; Darensbourg, M. Y. Coordination sphere flexibility of active-site models for Fe-only hydrogenase: studies in intra- and intermolecular diatomic ligand exchange. *J. Am. Chem. Soc.* **2001**, *123*, 3268−3278.
(74) Dzik, W. I.; van der Vlugt, J. I.; Reek, J. N. K.; de Bruin, B. Ligands that store and release electrons during catalysis. *Angew. Chem., Int. Ed.* **2011**, *50*, 3356−3358.
(75) Crabtree, R. H. Multifunctional ligands in transition metal catalysis. *New J. Chem.* **2011**, *35*, 18−23.
(76) Thammavongsy, Z.; Seda, T.; Zakharov, L. N.; Kaminsky, W.; Gilbertson, J. D. Ligand-based reduction of CO_2 and release of CO on Iron(II). *Inorg. Chem.* **2012**, *51*, 9168−9170.
(77) Silvia, J. S.; Cummins, C. C. Ligand-based reduction of CO_2 to CO mediated by an anionic niobium nitride complex. *J. Am. Chem. Soc.* **2010**, *132*, 2169−2171.
(78) Du, Y.; Yang, H.; Zhu, C.; Ortiz, M.; Okochi, K. D.; Shoemaker, R.; Jin, Y.; Zhang, W. Highly active multidentate ligand-based alkyne metathesis catalysts. *Chem. - Eur. J.* **2016**, *22*, 7959−7963.
(79) Zhao, C.; Crimmin, M. R.; Toste, F. D.; Bergman, R. G. Ligand-based carbon−nitrogen bond forming reactions of metal dinitrosyl complexes with alkenes and their application to C−H bond functionalization. *Acc. Chem. Res.* **2014**, *47*, 517−529.
(80) Wang, K.; Stiefel, E. I. Toward separation and purification of olefins using dithiolene complexes: an electrochemical approach. *Science* **2001**, *291*, 106−109.
(81) (a) Zarkadoulas, A.; Field, M. J.; Papatriantafyllopoulou, C.; Fize, J.; Artero, V.; Mitsopoulou, C. A. Experimental and theoretical insight into electrocatalytic hydrogen evolution with nickel bis-(aryldithiolene) complexes as catalysts. *Inorg. Chem.* **2016**, *55*, 432−444. (b) Zarkadoulas, A.; Field, M. J.; Artero, V.; Mitsopoulou, C. A. Proton-reduction reaction catalyzed by homoleptic nickel−bis-1,2-dithiolate complexes: experimental and theoretical mechanistic investigations. *ChemCatChem* **2017**, *9*, 2308−2317.
(82) Koshiba, K.; Yamauchi, K.; Sakai, K. A nickel dithiolate water reduction catalyst providing ligand-based Proton-Coupled Electron-Transfer pathways. *Angew. Chem., Int. Ed.* **2017**, *56*, 4247−4251.
(83) Yoshida, M.; Masaoka, S.; Sakai, K. Oxygen evolution from water catalyzed by mononuclear ruthenium complexes with a triazamacrocyclic ligand in a facial fashion. *Chem. Lett.* **2009**, *38*, 702−703.

DOI: 10.1021/acs.inorgchem.7b01954
Inorg. Chem. 2017, 56, 13852−13864